Optimal Design for Ultra-Broad-Band Amplifier

Xueming Liu and Byoungho Lee, *Senior Member, IEEE, Member, OSA*

***Abstract*—We propose a novel hybrid genetic algorithm (GA) based on such techniques as clustering, sharing, crowding, and adaptive probability. The proposed GA can effectively solve multimodal optimization, including the global and local optima in the distributed multipump Raman amplifier (DMRA). The simulation results show that the optimal signal bandwidth $\Delta\lambda$ can be evidently broadened by means of increasing the number of pumps and that $\Delta\lambda$ decreases with the increase of Raman gain and the improvement of the flatness property. The optimal results show that the hybrid erbium-doped fiber amplifier and DMRA can availably overcome the weakness of pure DMRA and that both higher gain and broader bandwidth can be realized in hybrid amplifiers simultaneously.**

***Index Terms*—Erbium-doped fiber amplifier (EDFA), genetic algorithm (GA), global optimization, multimodal optimization, Raman fiber amplifier, Raman scattering.**

I. Introduction

WAVELENGTH-DIVISION multiplexing (WDM) based on fiber amplifiers provides a transmission platform for the optical fiber communication systems and networks. Although the erbium-doped fiber amplifier (EDFA) has been utilized in WDM systems since the 1980s, almost every long-haul or ultra-long-haul fiber-optic transmission system recently uses Raman amplifiers or hybrid Raman/EDFAs [1]–[5]. By appropriately choosing wavelengths and powers of pump waves, Raman fiber amplifiers can provide broader amplification bandwidth and flexible center wavelength compared with pure EDFAs. Distributed multipump Raman amplifiers (DMRAs) help to significantly improve the noise characteristics, to realize longer transmission distances, and to upgrade existing systems [1]–[12]. In addition, the DMRA can mitigate fiber nonlinear effects and improve the optical signal-to-noise ratio without the need to increase the input optical signal power [1], [6].

In principle, the DMRA can obtain the arbitrary gain spectra by the proper choice of pump wavelengths and powers. However, the strong Raman interactions of pump-to-pump, signal-to-signal, and pump-to-signal make the problem of the required gain spectra become somewhat difficult for the optimal design of DMRA. Therefore, the DMRA design presents a grand challenge to numerical optimization. It involves multiple powers and wavelengths.

Another exciting development in Raman technology is the conjunction with EDFA to form hybrid amplifiers, especially when the system capacity needs to be upgraded by increasing the bandwidth expansion without raising channel speed [2]–[4]. When designed together, the EDFA and Raman amplifier offer better noise performance and pump efficiency than each separate amplifier [2]–[5].

The genetic algorithm (GA) is a global optimization method, which mimics the natural evolution and natural genetics. It has been successfully applied to finding the global optimum in a variety of unimodal domains. Unfortunately, a traditional GA tends to converge toward a single solution due to selection pressure, selection noise, and operator disruption [13]. However, some problems require the identification of multiple optima in the domains, or even multiple best peaks are equally meaningful. For this purpose, some methods such as the K-means algorithm, clustering, sharing, and crowding are proposed to extend the traditional GA to solve multimodal function optimization by forcing a GA to maintain a diverse population of members throughout its research [14]–[19].

Recently, although some methods [20]–[22] have been proposed to select the appropriate wavelengths and pump powers in Raman fiber amplifiers, their results are far from optimization [23]. Perlin and Winful employ GA to optimize the gain-flatness and gain-bandwidth performance. The optimal results are exciting, but they only obtain a single optimal solution in each domain [23], [24], and even their methods may be trapped in local optima of the search space due to the intrinsic weakness of the traditional GA (see the proof in Section IV). In [25], employing the neural network method optimizes the Raman-gain spectrum. However, it only partly obtains the optimization in pump power excluding wavelengths. We reported a hybrid GA for optimizing the DMRA design in [26]. This hybrid GA is modified in this paper, and then its searching ability is improved. In addition, we obtain the optimal results of bandwidth versus pump number, flatness, and gain, and we compare pure DMRA with hybrid EDFA/DMRA. These results can be extremely helpful in the real design of the DMRA.

This paper is organized as follows. In Section II, a novel hybrid genetic algorithm is proposed. The mathematical model for DMRA is given in Section III. A function is applied to testify our proposed GA in Sections IV. In Section V, the proposed algorithm is applied to a pure Raman amplifier and hybrid EDFA/DMRA, and some optimal results are obtained.

II. Hybrid Genetic Algorithm

GAs can establish objective functions without difficulty, regardless of whether the information comes from a simple equation or a very complex model [13], [27]. To identify multiple optima in multimodal domains, various population diversity mechanisms have been proposed. For example, sharing and crowding are two best-known niching techniques, which can maintain

Manuscript received April 30, 2003; revised August 14, 2003. This work was supported by the Ministry of Education of Korea under the Brain Korea 21 (Information Technology) Program.

The authors are with the School of Electrical Engineering, Seoul National University, 151-744 Seoul, Korea (e-mail: liuxueming72@yahoo.com; byoungho@snu.ac.kr).

Digital Object Identifier 10.1109/JLT.2003.820041

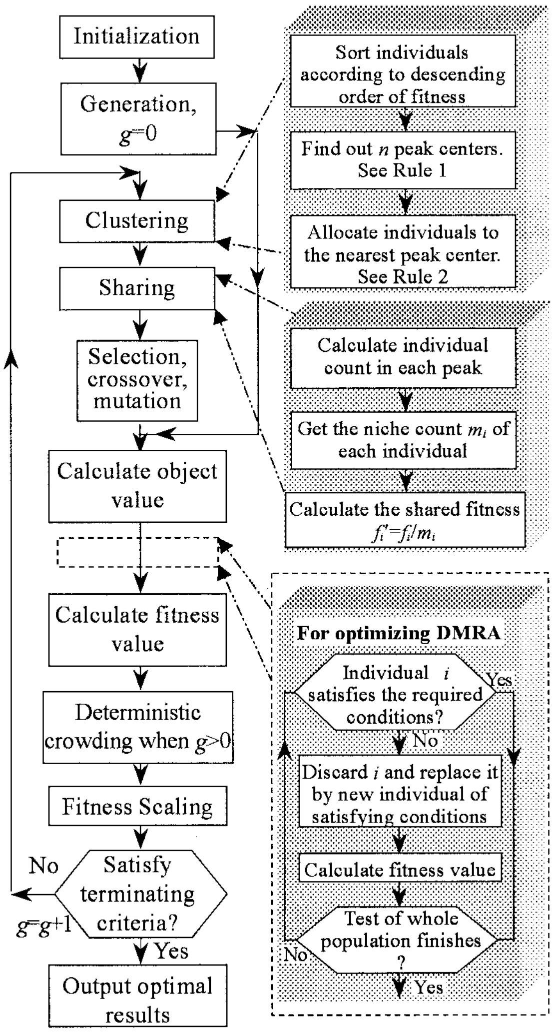

Fig. 1. Flowchart for our proposed GA.

many individuals in proportion to their fitness [13], [16]. Adaptive probabilities of crossover and mutation and adaptive genetic operators are employed to modify traditional GA [28], [29]. Clustering method provides a viable way to avoid local extrema, and it is a popular unsupervised pattern classification technique which partitions the input space into K regions based on some similarity/dissimilarity metric.

Based on the hybrid GA in [26], a modified hybrid GA is shown in Fig. 1. This GA employs such techniques as clustering, sharing, crowding, adaptive genetic operators, and fitness scaling. The main parts of the proposed GA are given as follows.

A. Initialization, Clustering, Sharing, and Crowding

In the initialization, one initializes the number of peak center n, the shortest niche radius r, and the number k; generates N individuals randomly; and sets the number of generation $g = 0$. The procedure of clustering is demonstrated in Fig. 1, and Rules 1 and 2 are shown in [26].

Each peak can be considered as a niche in the multimodal domain. Sharing, one of niching techniques, can maintain population diversity effectively. The shared fitness f_i' of an individual i is given by $f_i' = f_i/m_i$, where f_i is the genuine fitness and m_i is the niche count. m_i is equal to the individual count in the peak of individual i. The deterministic crowding is employed in our GA. Its detailed description is shown in [16].

B. Selection, Crossover, and Mutation

Selection, crossover, and mutation are based on the traditional GA. There are two essential characteristics in GA for optimizing multimodal functions. One is to converge to an optimum and the other is to explore new regions of the search space. By varying the crossover and mutation operators adaptively, the tradeoff between the exploration and exploitation can be obtained [28]. Srinivas and Patnaik had proposed adaptive crossover and mutation operators, which can prevent the premature convergence effectively [28]. However, their approach leads the best individual in the population to the undisrupted transfer into the next generation. In fact, it does not agree with the natural evolution. Therefore, we employ novel crossover and mutation operators, i.e., all individuals will have chances to reproduce the offspring generations with adaptive probabilities of crossover and mutation. That is

$$p_c = \begin{cases} p_{ch} - (p_{ch} - p_{cl}) \\ \quad \times (f_{m2} - f_{\text{ave}})/(f_{\max} - f_{\text{ave}}), & \text{if } f_{m2} > f_{\text{ave}} \\ p_{ch}, & \text{otherwise} \end{cases} \quad (1)$$

$$p_m = \begin{cases} p_{mh} - (p_{mh} - p_{ml}) \\ \quad \times (f - f_{\text{ave}})/(f_{\max} - f_{\text{ave}}), & \text{if } f > f_{\text{ave}} \\ p_{mh}, & \text{otherwise} \end{cases} \quad (2)$$

where p_c, p_{ch}, and p_{cl} are the probability of adaptive crossover, highest crossover, and lowest crossover; and p_m, p_{mh}, and p_{ml} are the probability of adaptive mutation, highest mutation, and lowest mutation, respectively. $f_{\max}$ and f_{ave} are the maximum fitness and average fitness of the entire population, respectively. f_{m2} is the maximum fitness of the two chromosomes being crossed, and f is the fitness of the chromosome.

To prevent GA from being trapped in local optima, we use the average finesses to extend the search space for the region containing the global optimum and assign $p_{ch} = 0.99$ and $p_{mh} = 0.02$. These ensure that almost all solutions with a fitness value no more than f_{ave} should undergo the crossover and mutation completely. When the fitness value approaches $f_{\max}$, the probabilities p_c and p_m are the lowest values of $p_{cl} = 0.7$ and $p_{ml} = 0.005$.

C. Fitness Scaling

GA chooses individuals randomly in terms of the fitness values of individuals, and the optimization procedure is based on the fitness function that is created by the objective function and the restrictive conditions. Thus, the fitness function is the most crucial aspect of GA, and usually it is designed to select the best individual in the region where all the constraints are satisfied. However, the domination of "superindividuals" in the population can cause the GA to converge prematurely. One way to improve sharing efficiency is to use fitness scaling [27]. A good fitness scaling can both maintain the diversity among optima and prevent premature convergence due to "superindividuals."

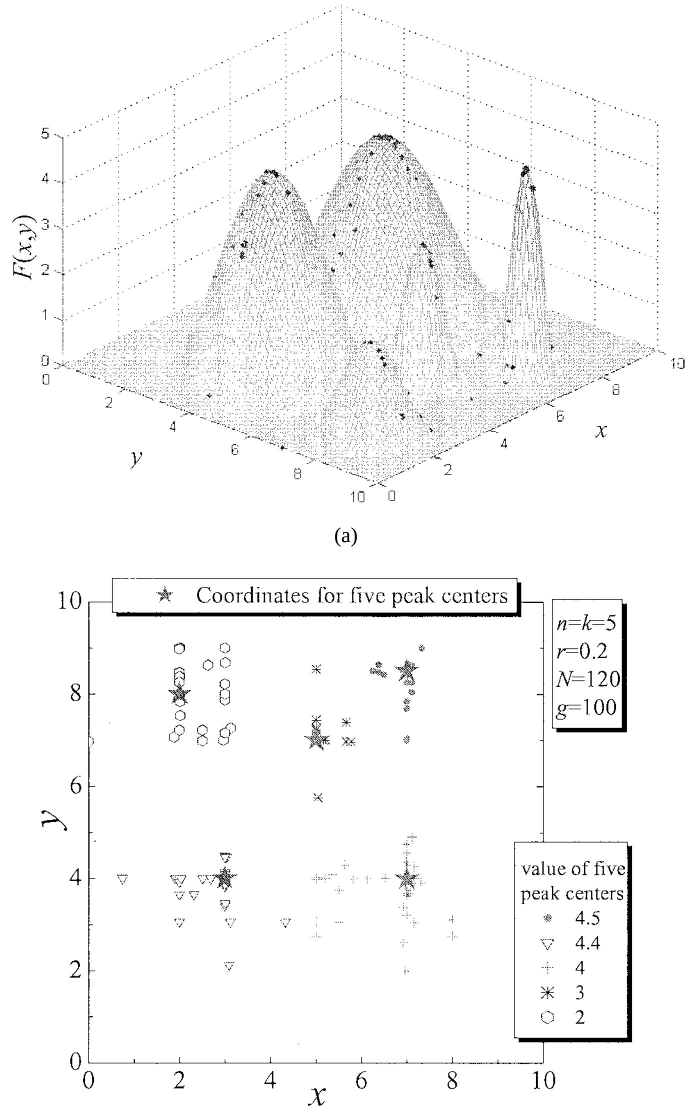

Fig. 2. Test function $F(x, y)$ and the entire population in the last generation (a) for the three-dimension figure of $F(x, y)$ and the distribution of all individuals after our proposed GA and (b) for the projection of all individuals of (a) in the xy plane. Five different symbols in (b) represent the individuals of five peak centers, respectively.

The most common scaling paradigm, called linear scaling, requires a linear relationship between raw fitness f and scaled fitness f'. This relationship is as follows [27]:

$$f' = a \cdot f + b \tag{3}$$

and

$$\begin{cases} \begin{cases} a = (C_m - 1) f_{\text{ave}} (f_{\max} - f_{\text{ave}}) \\ b = (f_{\max} - C_m f_{\text{ave}}) \\ \quad \times f_{\text{ave}} (f_{\max} - f_{\text{ave}}) \end{cases}, & \text{if } f_{\min} > \frac{C_m f_{\text{ave}} - f_{\max}}{C_m - 1} \\ \begin{cases} a = f_{\text{ave}} (f_{\text{ave}} - f_{\min}) \\ b = -a \cdot f_{\min} \end{cases}, & \text{otherwise} \end{cases} \tag{4}$$

where C_m is the number of expected copies desired for the best population member and the typical value of C_m is from 1.2 to 2. $C_m = 1.2$ in our simulation; $f_{\min}$ is the minimum fitness of the entire population; other parameters are the same as in (1) and (2). In (3) and (4), the raw and scaled fitness averages are kept equal, and the minimum raw fitness is mapped to a scaled fitness of zero.

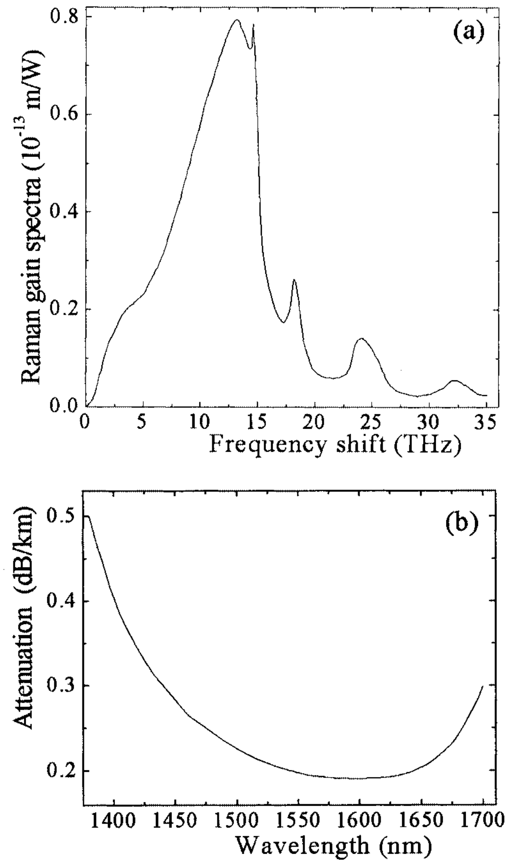

Fig. 3. Raman gain spectrum $g_R(\Delta v)$ of the fiber, and its attenuation spectrum $\alpha(v)$ in the window of 1400–1700 nm, for (a) $g_R(\Delta v)$ and (b) $\alpha(v)$.

D. For the Optimization of DMRA

In the optimization of DMRA, the dashed frame part in the right of Fig. 1 will be inserted in the flowchart. This part is critical for optimizing DMRA and is directional to all parameter set of DMRA. For meeting the required conditions of DMRA, every individual is checked, compared, and revised in this part.

Other parts in the flowchart are the same as the traditional GA.

III. Mathematical Model for DMRA

In the Raman amplifiers, stimulated Raman scattering (SRS) can lead to the energy exchange between forward- and backward-propagating waves. Because the power of backscattering pumps and signals is lower by ~30 dB and ~20 dB than the original power, and the power of forward and backward noises is less than that of input signals by ~30 dB [30], [31], such noise effects as spontaneous Raman scattering, Rayleigh backscattering, and thermal factor are skimmed in calculating the amplifier gain profile. Therefore, the major influence for designing the bandwidth of DMRA is the interactions of pump-to-pump, signal-to-signal, and pump-to-signal, as well as the attenuation.

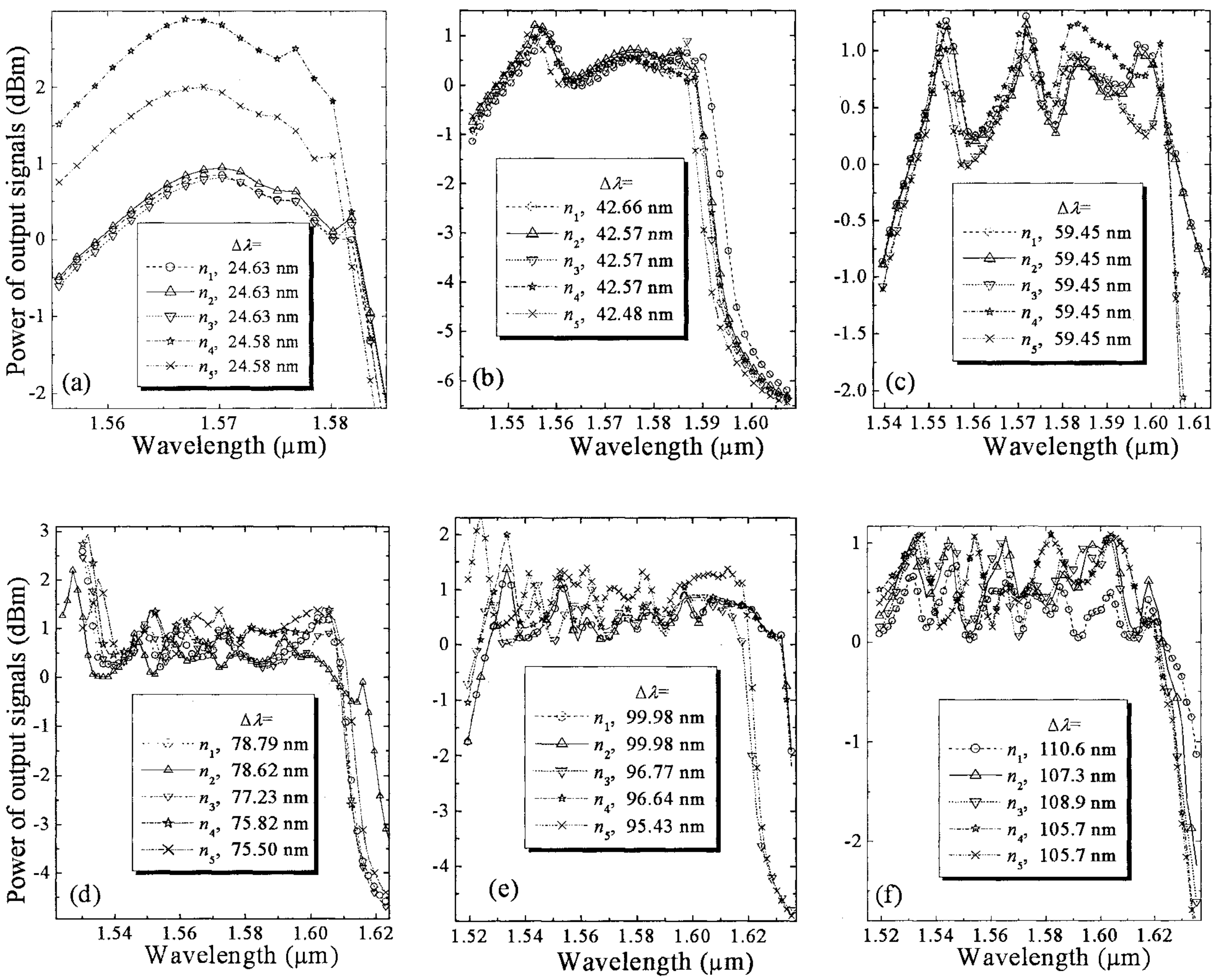

Fig. 4. Relationship between power of output signals and their wavelengths for (a) two pumps, (b) three pumps, (c) four pumps, (d) five pumps, (e) six pumps, and (f) seven pumps, respectively. The corresponding optimal values for power and wavelengths of pumps in (a)–(f) are tabularized in Tables I–VI, respectively. $n_i (i = 1, \ldots, 5)$ in figures and tables represents the ith peak center, and $\Delta\lambda$ is the optimal bandwidth for signals under the limiting conditions.

In the steady state, the coupled equation is described by [23], [24]

$$\pm \frac{dP_i}{dz} = \left[-\alpha(v_i) + \sum_{j=1}^{i-1} \frac{g_R(v_j - v_i)}{\Gamma A_{\text{eff}}} P_j - \sum_{j=i+1}^{m} \frac{v_i}{v_j} \frac{g_R(v_i - v_j)}{\Gamma A_{\text{eff}}} P_j \right] P_i, \quad (i = 1, 2, \ldots, m) \tag{5}$$

where P_i, v_i, and α_i are the power, frequency, and attenuation coefficient for the ith wave, respectively; A_{eff} is the effective area of optical fiber; the factor of Γ accounts for polarization randomization effects, whose value lies between 1 and 2; and $g_R(v_j - v_i)$ is the Raman gain coefficient from wave j to i. The frequency ratio v_i/v_j describes vibrational losses. The minus and plus signs on the left-hand side describe the backward-propagating pump waves and forward-propagating signal waves, respectively. The frequencies v_i are numerated in decreasing order of frequency $(i = 1, 2, \ldots, m)$. Terms from $j = 1$ to $j = i - 1$ and from $j = i + 1$ to $j = m$ cause amplification and attenuation of the channel at frequency v_i, respectively.

IV. Test Function

Real optimization problems often require the identification of multiple optima, either global or local or both. Our hybrid GA can maintain population diversity and permit it to investigate multiple peaks (including global and local) in parallel and can prevent the GA from being trapped in local optima of the search space. To prove these points, we employ as an example the test function

$$F(x, y) = \begin{cases} \frac{H_i}{R_i^2} \overline{R}^2 \left(\frac{\overline{R}^2}{R_i^2} - 2 \right) + H_i, & \text{if } \overline{R}^2 < R_i^2,\ x \in [0, 10], \text{ and } y \in [0, 10] \\ 0, & \text{otherwise} \end{cases} \tag{6}$$

where $\overline{R}^2 = (x - x_{ci})^2 + (y - y_{ci})^2$ and c_i, R_i, and $H_i (i = 1, \ldots, 5)$ are some constants: $c_i = (x_{ci}, y_{ci}) = \{(2, 8), (3, 4),$

$(5,7),(7,8.5),(7,4)\}$, $R_i = \{1.5, 2.5, 1, 0.75, 3\}$, and $H_i = \{2, 4.4, 3, 4.5, 4\}$. This test function consists of five peaks (i.e., c_i is the ith center coordinate, R_i is the ith radius, H_i is the ith height, and $i = 1, 2, 3, 4, 5$), which are displayed in Fig. 2. The values of five peaks are 4.5 at (7, 8.5), 4.4 at (3, 4), 4 at (7, 4), 3 at (5, 7), and 2 at (2, 8). Fig. 2 shows that the area of the second highest peak is much larger than that of the global peak, and its local peak value of 4.4 is very close to the global peak value of 4.5. It results in being very difficult to find the global peak without a special technique.

Each point in Fig. 2 corresponds to each individual in the last generation of GA a) for the three-dimensional figure of $F(x,y)$ and the distribution of all individuals after our proposed GA and b) for the projection of all individuals of Fig. 2(a) in the xy plane. Five different symbols in Fig. 2(b) represent the individuals of five peak centers, respectively. In the calculation, $n = k = 5$, $r = 0.2$, $N = 120$, and $g = 100$. Fig. 2 shows that the individuals in our GA can be approximately uniformly distributed in each peak [Fig. 2(b)]. The simulation results also show that our GA can find all five peaks in each calculation, but that the traditional GA usually finds the second highest peak. Therefore, our proposed hybrid GA can effectively solve multimodal optimal problems and escape from being trapped in local optima of the search space.

In addition, the numerical simulation also proves that the computing time T of our GA is obviously shortened by comparison with the traditional sharing GA. The reason is that $T \propto (kN)$ for our GA, but $T \propto (N^2)$ for the traditional sharing GA [27].

V. Numerical Simulation and Results

A. Initialization and Definition

To optimize pump spectra (i.e., wavelength and power), we apply the hybrid GA to calculate directly (5) instead of the multistage method of [23] and [24]. The detailed procedure is shown in the following. In *Initialization* of Fig. 1, first we define the range of every pump wavelength, which consists of fixed range and variable range. The variable range of pump wavelength is coded into the chromosome of GA, which is optimized in each generation (i.e., iteration step). Second, we define the range of each backward-propagating pump[1] power at $z = 0$, whose initial value is calculated from the algorithm of [31]. Finally, each pump spectrum (i.e., wavelength and power) and variable range are coded into the chromosome of individual. In the part of optimizing DMRA of each generation (see the dashed frame of Fig. 1), each individual is checked. If one individual does not satisfy the required conditions (e.g., gain and relative gain flatness F_{RG}), it is discarded and is replaced by a new individual satisfying the required conditions, which is coded from the demands of *Initialization*.

The relative gain flatness F_{RG} is defined as [24]

$$F_{\mathrm{RG}} = \frac{\Delta G}{(G_{\mathrm{on-off}})_{\min}} \tag{7}$$

where ΔG (dB) is the gain ripple, i.e., the difference between the maximal gain $(G_{\mathrm{on-off}})_{\max}$ and the minimal gain

TABLE I
POWER, WAVELENGTH, AND BANDWIDTH OF FIVE PEAK CENTERS FOR TWO PUMPS IN FIG. 4(a). $n_i (i = 1, \ldots, 5)$ ACCOUNTS FOR THE ith PEAK CENTER AND $\Delta\lambda$ IS THE OPTIMAL BANDWIDTH

	two pump power P_j (mW) and their wavelength λ_j (nm)				$\Delta\lambda$
	P_1	λ_1	P_2	λ_2	(nm)
n_1	82.11	1465.00	320.29	1468.52	24.63
n_2	79.44	1464.95	326.57	1468.97	24.63
n_3	75.87	1464.86	324.55	1469.14	24.63
n_4	203.83	1464.87	289.84	1467.94	24.58
n_5	119.90	1464.10	334.69	1467.46	24.58

TABLE II
POWER, WAVELENGTH, AND BANDWIDTH OF FIVE PEAK CENTERS FOR THREE PUMPS IN FIG. 4(b). $n_i (i = 1, \ldots, 5)$ ACCOUNTS FOR THE ith PEAK CENTER AND $\Delta\lambda$ IS THE OPTIMAL BANDWIDTH

	three pump power P_j (mW) and their wavelength λ_j (nm)						$\Delta\lambda$
	P_1	λ_1	P_2	λ_2	P_3	λ_3	(nm)
n_1	197.83	1448.14	52.62	1473.52	260.41	1476.44	42.66
n_2	195.73	1446.73	80.97	1471.28	241.21	1474.81	42.57
n_3	189.83	1447.03	203.28	1473.25	112.63	1473.94	42.57
n_4	189.28	1446.90	43.67	1469.00	274.96	1474.41	42.57
n_5	192.01	1445.34	184.36	1471.49	134.99	1473.41	42.48

TABLE III
POWER, WAVELENGTH, AND BANDWIDTH OF FIVE PEAK CENTERS FOR FOUR PUMPS IN FIG. 4(c). $n_i (i = 1, \ldots, 5)$ ACCOUNTS FOR THE ith PEAK CENTER AND $\Delta\lambda$ IS THE OPTIMAL BANDWIDTH

	four pump power P_j (mW) and their wavelength λ_j (nm)								$\Delta\lambda$
	P_1	λ_1	P_2	λ_2	P_3	λ_3	P_4	λ_4	(nm)
n_1	248.30	1444.11	160.63	1460.43	85.28	1482.38	150.39	1499.70	59.45
n_2	247.99	1444.23	160.60	1460.45	85.25	1482.28	152.91	1499.50	59.45
n_3	223.39	1442.70	126.01	1459.32	165.99	1486.48	86.23	1487.88	59.45
n_4	234.80	1443.12	130.24	1459.42	172.02	1486.08	85.68	1492.40	59.45
n_5	222.64	1442.81	125.72	1459.34	165.97	1486.38	85.29	1487.92	59.45

$(G_{\mathrm{on-off}})_{\min}[\Delta G = (G_{\mathrm{on-off}})_{\max} - (G_{\mathrm{on-off}})_{\min}]$. $G_{\mathrm{on-off}}$ (dB) is the ON-OFF (or gross) Raman gain, defined as [32]

$$G_{\mathrm{on-off}} = P(L) - P(0) + \alpha L \tag{8}$$

where $P(L)$ and $P(0)$ are the signal powers (dBm) at L and zero, respectively, and α is the attenuation coefficient. From (7) and (8), one can see that the relative gain flatness F_{RG} is a dimensionless value.

B. Parameters Set

In the numerical calculation, we employ the fast four-step method [31] and assume that $A_{\mathrm{eff}} = 80 \times 10^{-12} m^2, \Gamma = 2, L = 50$ km, $n = k = 5$, $r = 0.15$, $N = 600$, and $g = 1500$. The power of each channel is 1 mW, spaced by 200 GHz/channel. The gain spectrum $g_R(\Delta v)$ and attenuation spectrum $\alpha(v)$ of the fiber are shown in Fig. 3 [33].[2]

C. Optimized Results Between Bandwidth and Pump Number

Fig. 4 demonstrates the relationship between power of output signals and their wavelengths for a) two pumps, b) three pumps, c) four pumps, d) five pumps, e) six pumps, and f) seven pumps.

[1]The input port of pump is at $z = L$.

[2]http://syllabus.syr.edu/ELE/kdl/Ele682/smf28.PDF

TABLE IV
POWER, WAVELENGTH, AND BANDWIDTH OF FIVE PEAK CENTERS FOR FIVE PUMPS IN FIG. 4(d). $n_i (i = 1, \ldots, 5)$ ACCOUNTS FOR THE iTH PEAK CENTER AND $\Delta\lambda$ IS THE OPTIMAL BANDWIDTH

	five pump power P_j (mW) and their wavelength λ_j (nm)										$\Delta\lambda$
	P_1	λ_1	P_2	λ_2	P_3	λ_3	P_4	λ_4	P_5	λ_5	(nm)
n_1	518.77	1423.16	195.49	1440.06	91.05	1460.43	41.39	1488.89	63.80	1491.87	78.79
n_2	468.72	1421.60	194.95	1437.87	98.86	1456.29	61.51	1476.84	60.70	1498.20	78.62
n_3	471.58	1424.82	190.43	1441.06	102.00	1460.61	43.90	1490.17	69.57	1491.23	77.23
n_4	365.45	1428.18	210.35	1442.33	110.61	1459.94	65.09	1489.96	88.55	1493.56	75.82
n_5	516.58	1425.09	196.83	1442.46	75.17	1461.39	69.24	1488.67	53.58	1491.23	75.50

TABLE V
POWER, WAVELENGTH, AND BANDWIDTH OF FIVE PEAK CENTERS FOR SIX PUMPS IN FIG. 4(e). $n_i (i = 1, \ldots, 5)$ ACCOUNTS FOR THE iTH PEAK CENTER AND $\Delta\lambda$ IS THE OPTIMAL BANDWIDTH

	six pump power P_j (mW) and their wavelength λ_j (nm)												$\Delta\lambda$
	P_1	λ_1	P_2	λ_2	P_3	λ_3	P_4	λ_4	P_5	λ_5	P_6	λ_6	(nm)
n_1	417.70	1426.47	250.54	1443.91	101.74	1462.66	64.31	1481.69	13.40	1502.06	50.86	1511.40	99.98
n_2	418.16	1426.27	250.71	1443.80	101.75	1462.64	64.31	1481.78	13.11	1502.26	50.87	1511.69	99.98
n_3	329.52	1420.81	251.97	1436.00	142.11	1453.10	66.42	1470.41	29.97	1495.11	64.38	1499.33	96.77
n_4	475.38	1426.27	239.40	1443.80	96.20	1462.64	66.51	1481.78	11.43	1502.26	44.74	1511.06	96.64
n_5	571.25	1418.39	236.90	1433.54	135.11	1451.23	87.86	1469.49	31.96	1499.54	25.08	1501.01	95.43

TABLE VI
POWER, WAVELENGTH, AND BANDWIDTH OF FIVE PEAK CENTERS FOR SEVEN PUMPS IN FIG. 4(f). $n_i (i = 1, \ldots, 5)$ ACCOUNTS FOR THE iTH PEAK CENTER AND $\Delta\lambda$ IS THE OPTIMAL BANDWIDTH

	seven pump power P_j (mW) and their wavelength λ_j (nm)														$\Delta\lambda$
	P_1	λ_1	P_2	λ_2	P_3	λ_3	P_4	λ_4	P_5	λ_5	P_6	λ_6	P_7	λ_7	(nm)
n_1	263.68	1424.11	235.29	1437.59	114.43	1455.03	69.47	1472.36	34.07	1487.19	30.09	1505.41	27.65	1511.14	110.6
n_2	260.29	1425.08	249.56	1436.89	152.03	1452.72	47.66	1471.85	45.00	1487.02	33.29	1501.19	37.92	1502.91	107.3
n_3	275.27	1424.27	264.02	1436.33	137.80	1454.88	47.19	1471.99	42.92	1487.46	30.93	1502.03	36.01	1503.82	108.9
n_4	144.09	1423.12	278.91	1428.47	220.07	1444.49	87.65	1466.96	48.52	1487.63	32.69	1501.05	32.56	1504.57	105.7
n_5	135.33	1423.12	294.00	1428.47	216.90	1444.49	87.10	1466.95	48.03	1487.64	32.07	1500.99	33.62	1504.10	105.7

In the numerical calculations, the wavelength of the center channel is given as 1575 nm, and the number of channels is 25, 41, 45, 57, 71, and 75 for two, three, four, five, six, and seven pumps, respectively. We also assume that the gross Raman gain can compensate the attenuation of signals (i.e., $G_{\text{on-off}} > \alpha L$, or the net gain is larger than zero), $F_{\text{RG}} < 0.1$, and the number of peak centers $n = 5$. After the numerical simulation based on our hybrid GA, the optimal results are plotted in Fig. 4(a)–(f) and their corresponding optimal values for power and wavelengths of pumps are tabularized in Table I–VI. $n_i (i = 1, \ldots, 5)$ in figures and tables represents the ith peak center, and $\Delta\lambda$ is the optimal signal bandwidth under the above conditions.

From Fig. 4 and Tables I–VI, one can see that:

1) there are the same or approximately the same $\Delta\lambda$'s for each peak center for a given pump number;
2) the maximum $\Delta\lambda$ increases with the addition of pump number, i.e., $\Delta\lambda$ is 24.63, 42.66, 59.45, 78.79, 99.98, and 110.6 nm for two, three, four, five, six, and seven pumps, respectively;
3) to realize the fixed $\Delta\lambda$ in the experiments, therefore, there are several candidates by the optimization of our GA, as has important applications in the design of DMRA;
4) our proposed GA can effectively avoid the local trap during the optimal procedure;
5) the global maximum value $\Delta\lambda$ lies in the first peak center n_1, as is determined in the assumption of our GA.

To more clearly understand the reaction between pumps and signals, the evolution of all channels transmitting along the fiber for the first peak center of six pumps [i.e., n_1 in Fig. 4(e)] is plotted in Fig. 5. It is easily found that, from Fig. 5:

1) there are strong interactions of signal-to-signal and pump-to-signal;
2) the pump-to-signal interaction can compensate the attenuation of signals and make signals increase when $z >\sim$ 30 km;
3) SRS effects of signal-to-signal make the power of higher frequency (i.e., shorter wavelength) waves flow into that of lower frequency (i.e., longer wavelength) waves.

D. Optimized Results for Bandwidth With ΔG and $G_{\text{on-off}}$

To reveal the influence of some major parameters on the DMRA bandwidth, we plotted the figures that show the relationships between $\Delta\lambda$ and ΔG or $G_{\text{on-off}}$ in Figs. 6 and 7, respectively. In calculating Fig. 6, we assumed that the channel number of signals is 65 and the net gain is more than zero (i.e., $G_{\text{on-off}} > \alpha L$). Fig. 6 shows the relationships of $\Delta\lambda$ with ΔG, and of power of output signals with their wavelengths, where (a)–(e) show five examples of (f) under the conditions

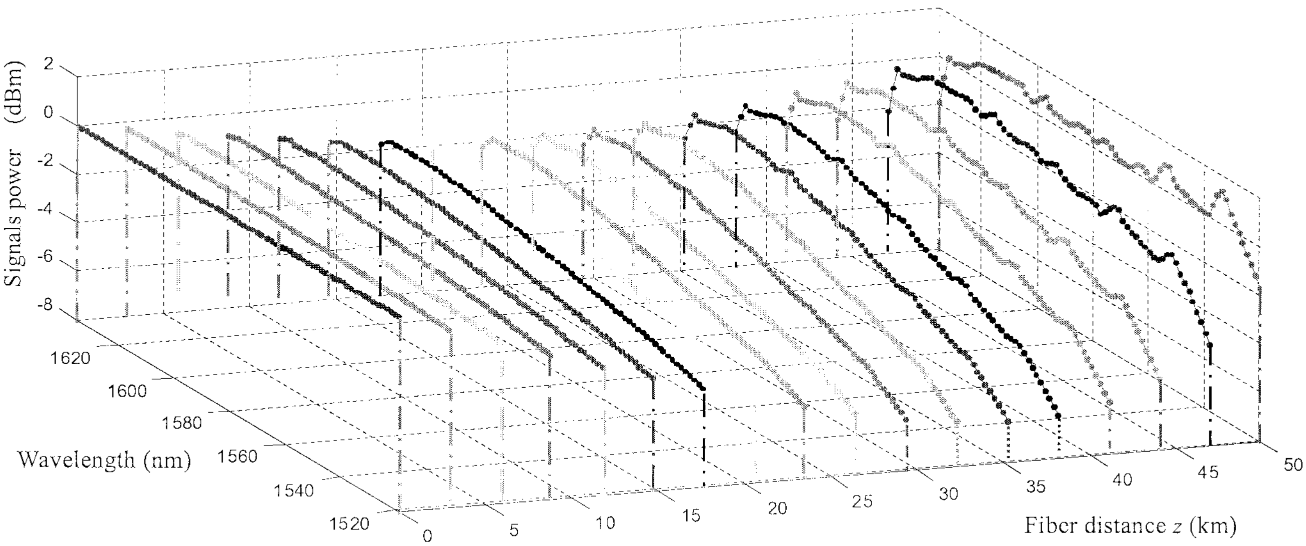

Fig. 5. Evolution of all channels transmitting along the fiber for the first peak center of six pumps, i.e., n_1 in Fig. 4(e).

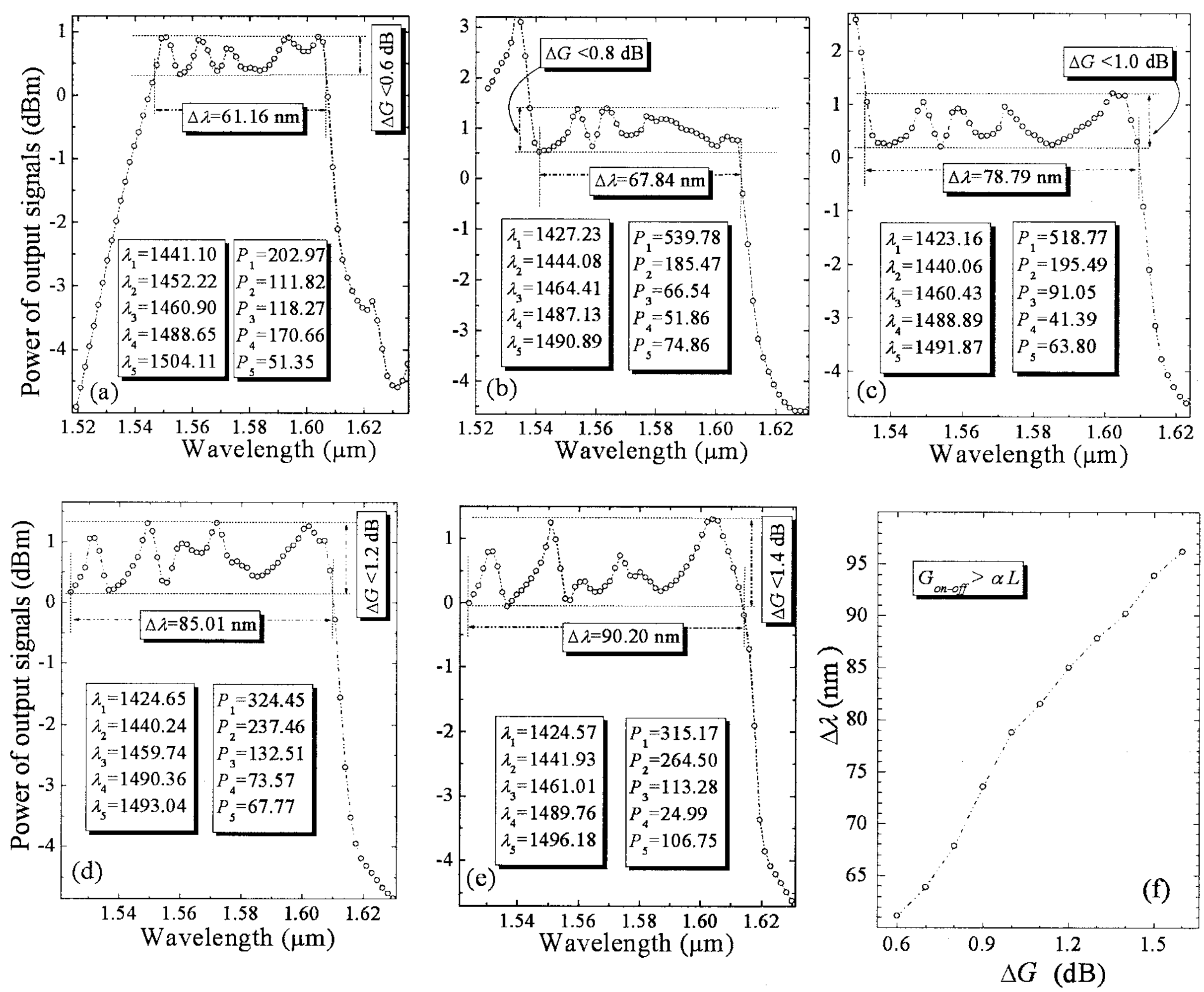

Fig. 6. Relationship of $\Delta\lambda$ with ΔG and of power of output signals with their wavelengths, where (a)–(e) show five examples of (f) under the conditions of $\Delta G < 0.6, 0.8, 1.0, 1.2,$ and 1.4 dB, respectively.

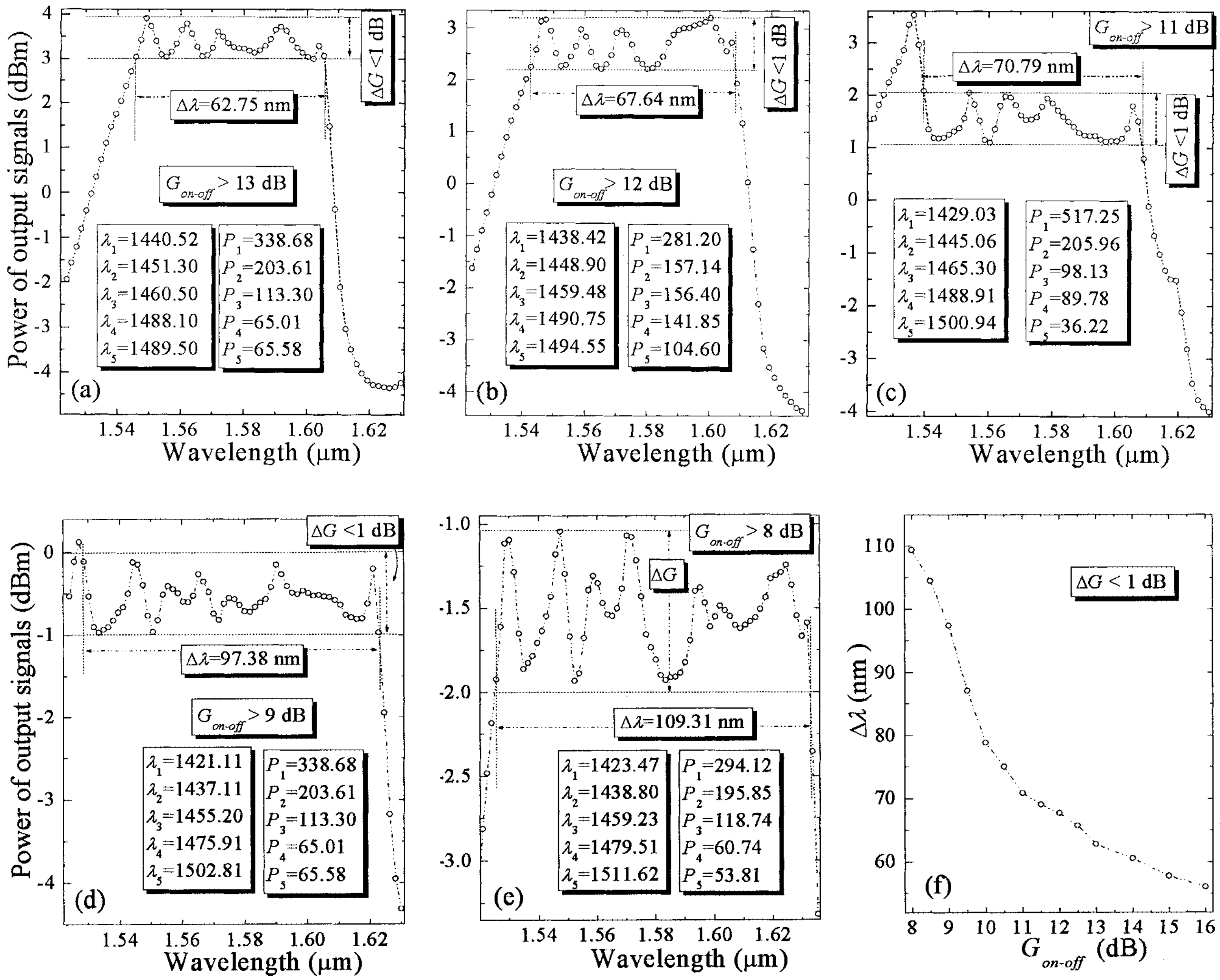

Fig. 7. Relationship of $\Delta\lambda$ with gross Raman gain (i.e., $G_{\text{on-off}}$) and power of output signals with their wavelengths, where (a)–(e) show five examples of (f) under the conditions of $G_{\text{on-off}} > 13, 12, 11, 9$, and 8 dB, respectively.

of $\Delta G < 0.6, 0.8, 1.0, 1.2$, and 1.4 dB, respectively. Fig. 7 exhibits the relationships of $\Delta\lambda$ with gross Raman gain (i.e., $G_{\text{on-off}}$) and of power of output signals with their wavelengths, where (a)–(e) show five examples of (f) under the conditions of $G_{\text{on-off}} > 8, 9, 11, 12$, and 13 dB, respectively. Additionally, the condition of $\Delta G < 1$ dB is assumed in calculating curves of Fig. 7. The units of power P and wavelength λ in legends of Figs. 6 and 7 are mW and nm, respectively.

From Fig. 6(f), one can find that $\Delta\lambda$ broadens with increase of ΔG. Five examples in Fig. 6(a)–(e) can describe these phenomena in more detail, i.e., $\Delta\lambda = 61.16, 67.84, 78.79, 85.01$, and 90.20 nm for $\Delta G < 0.6, 0.8, 1.0, 1.2$, and 1.4 dB, respectively. Therefore, increasing $\Delta\lambda$ is at the cost of decreasing the flatness property.

From Fig. 7(a)–(e), one can see that $\Delta\lambda$ is equal to 62.75, 67.64, 70.79, 97.38, and 109.31 nm under the conditions of $G_{\text{on-off}} > 13, 12, 11, 9$, and 8 dB, respectively. So, $\Delta\lambda$ decreases with the increase of gross Raman gain (i.e., $G_{\text{on-off}}$). The rule is shown in Fig. 7(f) more clearly. Figs. 6 and 7 show that, in pure DMRA, increasing the Raman gain and improving the flatness property lead to the decrease of $\Delta\lambda$. However, these shortcomings can be overcome in the following section, based on hybrid amplifiers (i.e., the combination of EDFA and DMRA).

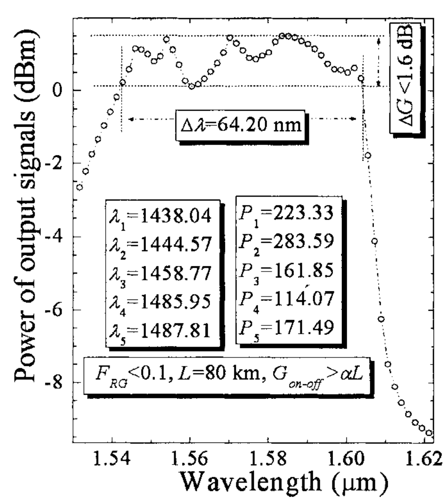

Fig. 8. Optimal results for pure DMRA.

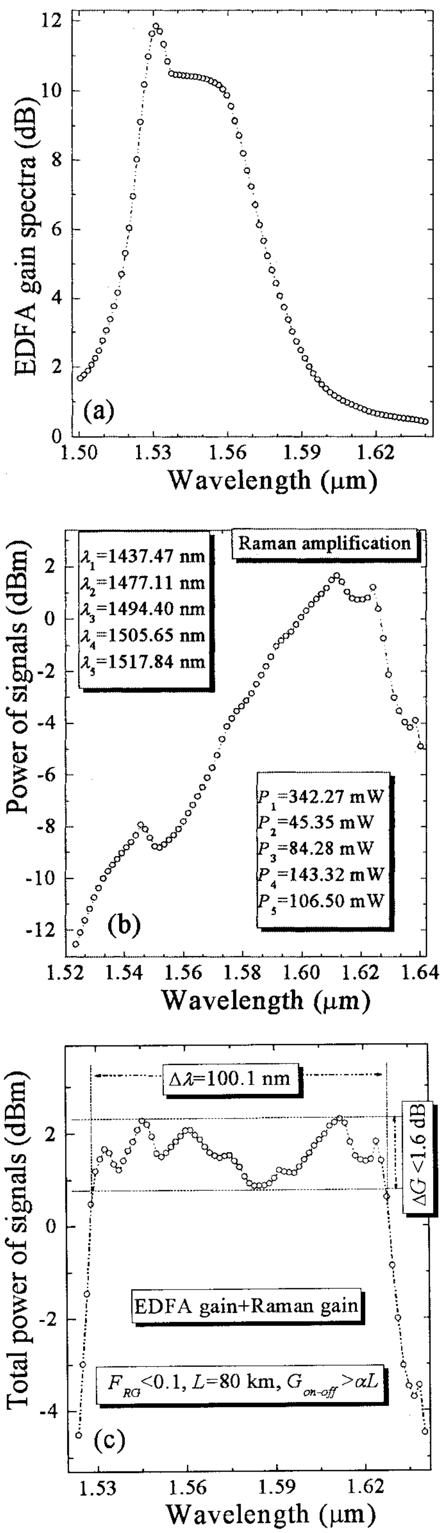

Fig. 9. EDFA gain spectra and optimal results for hybrid amplifier for (a) EDFA gain spectra, (b) pure Raman amplification, and (c) hybrid EDFA/DMRA amplification. The corresponding optimal values for power P and wavelength λ of pumps are included in the legend of (b).

E. Optimized Results for Hybrid Amplifier

Because EDFA can effectively amplify C-band [34] and increasing $G_{\text{on-off}}$ is at the cost of decreasing $\Delta\lambda$ for pure DMRA (see Fig. 7), hybrid amplifiers can overcome the individual shortcoming and obtain both broadband $\Delta\lambda$ and high gain. We optimize two examples, based on our proposed GA, to explain single and hybrid amplifiers. One is pure DMRA that is shown in Fig. 8, and the other is the hybrid amplifier demonstrated in Fig. 9. In the optimal simulations, we assume that the number of channels is 65, EDFA gain spectra is plotted in Fig. 9(a) [34], $L = 80$ km, $G_{\text{on-off}} > \alpha L$, and $F_{\text{RG}} < 0.1$. Figs. 8 and 9 illustrate the optimal results for pure DMRA and hybrid amplifiers. One can find, from Figs. 8 and 9, that:

1) $\Delta\lambda$ is 64.20 nm for pure DMRA but 100.1 nm for hybrid amplifier;
2) C-band channels are amplified mainly by EDFA, but L-band channels are done by DMRA;
3) hybrid amplifiers can obviously decrease the total pump power in the transmission fiber in comparison with pure DMRA, so the nonlinear effects (e.g., cross-phase modulation, four-wave mixing, etc.) can be mitigated greatly.

VI. Conclusion

A novel GA based on techniques such as clustering, sharing, crowding, and adaptive probability is proposed in this paper, for the first time to the authors' knowledge. A test function proves that our GA can obtain the global and all local peak values in parallel. Hence, the proposed GA can effectively solve the multimodal optimization (including the global and local optima) in DMRA. The simulation results show that the optimal signal bandwidth $\Delta\lambda$ can be effectively broadened by means of increasing the number of pumps, i.e., $\Delta\lambda$ is 24.63, 42.66, 59.45, 78.79, 99.98, and 110.6 nm for two, three, four, five, six, and seven pumps, respectively. $\Delta\lambda$ decreases with the improvement of flatness property and the increase of Raman gain, e.g., under the same conditions, $\Delta\lambda = 61.16, 67.84, 78.79, 85.01,$ and 90.20 nm for $\Delta G < 0.6, 0.8, 1.0, 1.2,$ and 1.4 dB; and $\Delta\lambda = 62.75, 67.64, 70.79, 97.38,$ and 109.31 nm for $G_{\text{on-off}} > 13, 12, 11, 9,$ and 8 dB in our optimal simulations, respectively. The optimal results of hybrid EDFA/DMRA amplifiers show that the weakness of pure DMRA can be availably overcome, and that both higher gain and broader bandwidth can be realized simultaneously. For instance, $\Delta\lambda$ is 64.20 and 100.1 nm for the pure DMRA and hybrid EDFA/DMRA under the conditions of $G_{\text{on-off}} > \alpha L$, $F_{\text{RG}} < 0.1$, $L = 80$ km, and the pump number of five.

Acknowledgment

The authors would like to thank Dr. X. Yu, Tsinghua University, for fruitful discussions on the GA.

References

[1] M. N. Islam, "Raman amplifiers for telecommunications," *IEEE J. Select. Topics Quantum Electron.*, vol. 8, pp. 548–559, 2002.
[2] S. Kawai, H. Masuda, K. Suzuki, and K. Aida, "Wide-bandwidth and long-distance WDM transmission using highly gain-flattened hybrid amplifier," *IEEE Photon. Technol. Lett.*, vol. 11, no. 7, pp. 886–888, 1999.
[3] H. Suzuki, J. Kani, H. Masuda, N. Takachio, K. Iwatsuki, Y. Tada, and M. Sumida, "1-Tb/s (100 × 10 Gb/s) super-dense WDM Transmission with 25-GHz channel spacing in the zero-dispersion region employing distributed Raman amplification technology," *IEEE Photon. Technol. Lett.*, vol. 12, no. 7, pp. 903–905, 2000.

[4] T. N. Nielsen, A. J. Stentz, K. Rottwitt, D. S. Vengsarkar, Z. J. Chen, P. B. Hansen, J. H. Park, K. S. Feder, S. Cabot, S. Stulz, D. W. Peckham, L. Hsu, C. K. Kan, A. F. Judy, S. Y. Park, L. E. Nelson, and L. Gruner-Nielson, "3.28-Tb/s transmission over 3 × 100 km nonzero-dispersion fiber using dual C- and L-band distributed Raman amplification," *IEEE Photon. Technol. Lett.*, vol. 12, no. 8, pp. 1079–1081, 2000.
[5] A. Carena, V. Curri, and P. Poggiolini, "On the optimization of hybrid Raman/erbium-doped fiber amplifiers," *IEEE Photon. Technol. Lett.*, vol. 13, no. 11, pp. 1170–1172, 2001.
[6] S. Namiki and Y. Emori, "Ultrabroad-band Raman amplifiers pumped and gain-equalized by wavelength-division-multiplexed high-power laser diodes," *IEEE J. Select. Topics Quantum Electron.*, vol. 7, pp. 3–16, 2001.
[7] T. Mizuochi, K. Kinjo, S. Kajiya, T. Tokura, and K. Motoshima, "Bidirectional unrepeatered 43 Gb/s WDM transmission with C/L band-separated Raman amplification," *J. Lightwave Technol.*, vol. 20, pp. 2079–2085, Dec. 2002.
[8] E. M. Dianov, "Advances in Raman fibers," *J. Lightwave Technol.*, vol. 20, pp. 1457–1462, Aug. 2002.
[9] M. Karásek and M. Menif, "Channel addition/removal response in Raman fiber amplifiers: modeling and experimentation," *J. Lightwave Technol.*, vol. 20, pp. 1680–1687, Sept. 2002.
[10] N. Kikuchi, K. K. Wong, K. Uesaka, K. Shimizu, S. Yam, E. S. Hu, M. Marhic, and L. G. Kazovsky, "Novel in-service wavelength-band upgrade scheme for fiber Raman amplifier," *IEEE Photon. Technol. Lett.*, vol. 15, pp. 27–29, Jan. 2003.
[11] H. Masuda, S. Kawai, K.-I. Suzuki, and K. Aida, "Ultrawide 75-nm 3-dB gain-band optical amplification with erbium-doped fluoride fiber amplifiers and distributed Raman amplifiers," *IEEE Photon. Technol. Lett.*, vol. 10, no. 4, pp. 516–518, 1998.
[12] H. Masuda and S. Kawai, "Wide-band and gain-flattened hybrid fiber amplifier consisting of an EDFA and a multiwavelength pumped Raman amplifier," *IEEE Photon. Technol. Lett.*, vol. 11, no. 6, pp. 647–649, Jun. 1999.
[13] S. W. Mahfoud, "Niching methods for genetic algorithms," Ph.D. dissertation, Univ. of Illinois, Urbana-Champaign, 1995.
[14] S. Bandyopadhyay and U. Maulik, "An evolutionary technique based on K-means algorithm for optimal clustering in R^N," *Inform. Sci.*, vol. 146, pp. 221–237, 2002.
[15] J. K Kim, D. H. Cho, H. K. Jung, and C. G. Lee, "Niching genetic algorithm adopting restricted competition selection combined with pattern search method," *IEEE Trans. Magn.*, vol. 38, no. 2, pp. 1001–1104, 2002.
[16] S. W. Mahfoud, "Crowding and preselection revisited," in *Parallel Problem Solving From Nature*, R. Manner and B. Manderick, Eds. Amsterdam, The Netherlands: Elsevier Science, 1992, vol. 2, pp. 27–36.
[17] B. L. Miller and M. J. Shaw, "Genetic algorithms with dynamic niche sharing for multimodal function optimization," in *Proc. 1996 IEEE Int. Conf. Evolutionary Computation*. Piscataway, NJ: IEEE Press, 1996, pp. 786–791.
[18] D. Thierens and D. E. Goldberg, "Elitist recombination: an integrated selection recombination GA," in *Proc. 1st IEEE Conf. Evolutionary Computation,* 1994, pp. 508–512.
[19] X. Yin and N. Germay, "A fast genetic algorithm with sharing scheme using cluster analysis methods in multimodal function optimization," in *Proc. Int. Conf. Innsbruck Artificial Neural Networks and Genetic Algorithms*, R. F. Albrecht, C. Reeves, and N. C. Steele, Eds. Berlin, Germany: Springer-Verlag, 1993, pp. 450–457.
[20] M. Yan, J. Chen, W. Jiang, J. Li, J. Chen, and X. Li, "Automatic design scheme for optical-fiber Raman amplifiers backward-pumped with multiple laser diode pumps," *IEEE Photon. Technol. Lett.*, vol. 13, pp. 948–950, 2001.
[21] X. Zhou, C. Lu, P. Shum, and T. H. Cheng, "A simplified model and optimal design of a multiwavelength backward-pumped Raman amplifier," *IEEE Photon. Technol. Lett.*, vol. 13, pp. 945–947, Sept. 2001.
[22] Y. Emori and S. Namiki, "Broadband Raman amplifier for WDM," *IEICE Trans. Electron.*, vol. E84-0C, pp. 593–597, Sept. 2001.
[23] V. E. Perlin and H. G. Winful, "Efficient design method for multi-pump flat-gain fiber Raman amplifiers," in *OFC'02*, 2002, pp. 57–59.
[24] ——, "Optimal design of flat-gain wide-band fiber Raman amplifiers," *J. Lightwave Technol.*, vol. 20, pp. 250–254, Feb. 2002.
[25] P. C. Xiao, Q. J. Zeng, J. Huang, and J. M. Liu, "A new optimal algorithm for multipump sources of distributed fiber Raman amplifier," *IEEE Photon. Technol. Lett.*, vol. 15, no. 2, pp. 206–208, 2003.
[26] X. M. Liu and B. Lee, "Optimal design of fiber Raman amplifier based on hybrid genetic algorithm," *IEEE Photon. Technol. Lett.*, vol. 16, Feb. 2004, to be published.
[27] D. E. Goldberg, *Genetic Algorithms in Search, Optimization, and Machine Learning*. New York: Addison-Wesley, 1989.
[28] M. Srinivas and L. M. Patnaik, "Adaptive probabilities of crossover and mutation in genetic algorithms," *IEEE Trans. Syst., Man, Cybern.*, vol. 24, pp. 656–667, Apr. 1994.
[29] F. Herrera and M. Lozano, "Adaptive genetic operators based on coevolution with fuzzy behaviors," *IEEE Trans. Evol. Comput.*, vol. 5, pp. 149–165, Apr. 2001.
[30] X. M. Liu, "Comments on 'A novel method for Raman amplifier propagation equations," *IEEE Photon. Technol. Lett.*, vol. 15, p. 1321, Sept. 2003.
[31] X. M. Liu and B. Lee, "A fast and stable method for Raman amplifier propagation equations," *Opt. Express*, vol. 11, no. 18, pp. 2163–2176, Sept. 2003.
[32] P. Kim, J. Park, H. Yoon, J. Park, and N. Park, "In situ design method for multichannel gain of a distributed Raman amplifier with multiwave OTDR," *IEEE Photon. Technol. Lett.*, vol. 14, no. 12, pp. 1683–1685, 2002.
[33] X. M. Liu and B. Lee, "Effective shooting algorithm and its application to fiber amplifiers," *Opt. Express*, vol. 11, no. 12, pp. 1452–1461, Jun. 2003.
[34] P. C. Becker, N. A. Olsson, and J. R. Simpson, *Erbium-Doped Fiber Amplifiers: Fundamentals and Technology*. London, U.K.: Academic, 1999.

Xueming Liu was born in Hunan Province, China, in 1972. He received the B.S. degree from the Department of Physics, Xiangtan Normal University, Xiangtan, China, in 1994 and the M.S. and Ph.D. degrees from the Department of Electronic Engineering, Southeast University, Nanjing, China, in 1997 and 2000, respectively.

From 2000 to 2002, he engaged in postdoctoral research at Tsinghua University, Beijing, China. He is currently engaged in postdoctoral work at the School of Electrical Engineering, Seoul National University, Seoul, Korea. His current research interests lie in nonlinear optics, optical fiber communication systems and networks, nonlinearities in the optical communication network, and photonic crystal. He has published more than 40 papers.

Byoungho Lee (M'94–SM'00) received the B.S. and M.S. degrees in electronics engineering from Seoul National University, Seoul, Korea, in 1987 and 1989, respectively, and the Ph.D. degree in electrical engineering and computer science from the University of California at Berkeley in 1993.

In 1994, he joined the Faculty of the School of Electrical Engineering, Seoul National University, where he is now an Associate Professor. He has authored or coauthored more than 100 international journal papers and more than 170 international conference papers. His research fields are optical fiber devices, three-dimensional display, and hologram applications.

Prof. Lee is a Fellow of The International Society for Optical Engineers (SPIE) and a Member of the Optical Society of America (OSA). In 1999, his laboratory was honored as a National Research Laboratory by the Ministry of Science and Technology of Korea. In 2002, he received the Presidential Young Scientist Award of Korea.